Atmospheric
Chemistry
and Physics

Supplement of

Measurement report: Rapid changes of chemical characteristics and health risks for highly time resolved trace elements in PM$_{2.5}$ in a typical industrial city in response to stringent clean air actions

Rui Li et al.

Correspondence to: Rui Li (rli@geo.ecnu.edu.cn), Meng Peng (mvponesky@163.com), and Weidong Zhao (zhaoweidong@ccidthinktank.com)

Detailed clean air actions in China since 2013

Since 2013, the Chinese government imposed many emission controls to alleviate the air pollution across China. First of all, the government department enhanced a comprehensive air pollution control on industrial enterprises, non-point source control, and vehicle pollution control (Ma et al., 2019). Secondly, many industrial enterprises were required to upgrade their industrial structure, to control new capacity with high energy consumption and to accelerate the elimination of backward production capacity (Li et al., 2021). Thirdly, the energy structure adjustment and utilization of clean energy were also accelerated. The fossil fuel consumption also has been strictly controlled and it was tried to improve the energy efficiency (Ma et al., 2019). In addition, the Chinese governments tried to optimize the industrial layout (Ma et al., 2019). The Chinese government also established the market mechanisms to improve pricing and tax policy (Li et al., 2021). At last, many monitoring sites were constructed across China to investigate the near-time air pollution and the joint prevention and control measures were also enhanced.

Figure S1 Monthly average values of WS (m/s), T (℃), relative humidity (RH) (%) and air pressure (P) (hPa) during the sampling period. The blue, green, orange, and pink bobbles denote WS, T, RH, and P, respectively.
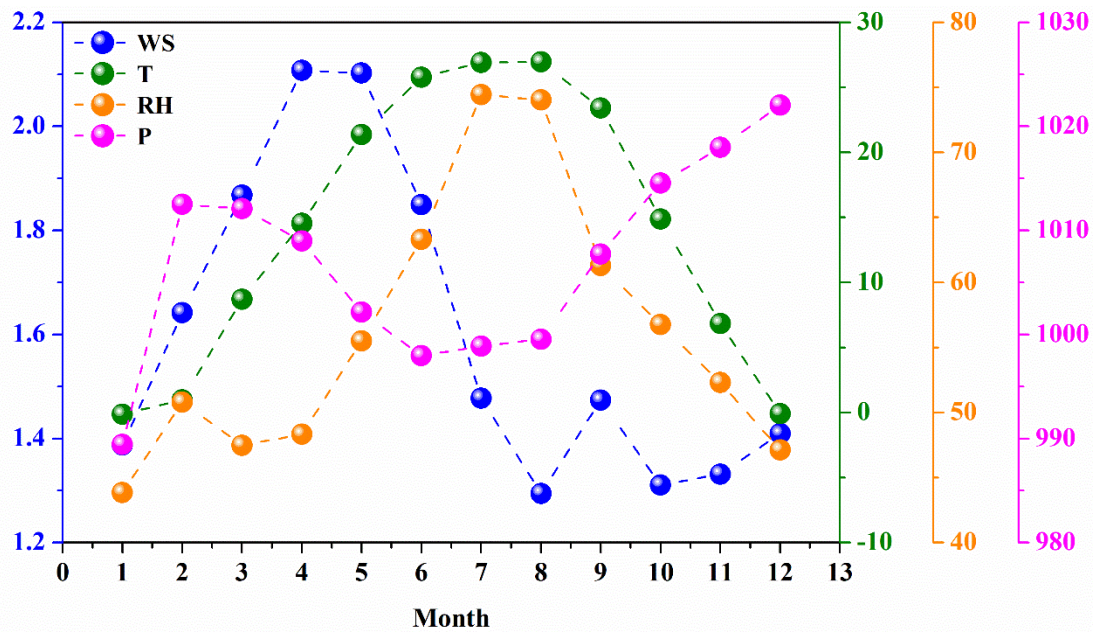
Figure S2 Time-series for Ag (a), As (b), Ca (c), Co (d), Cr (e), Cu (f), Fe (g), and Ga (h) during 2017-2020 (Unit: ng/m³).
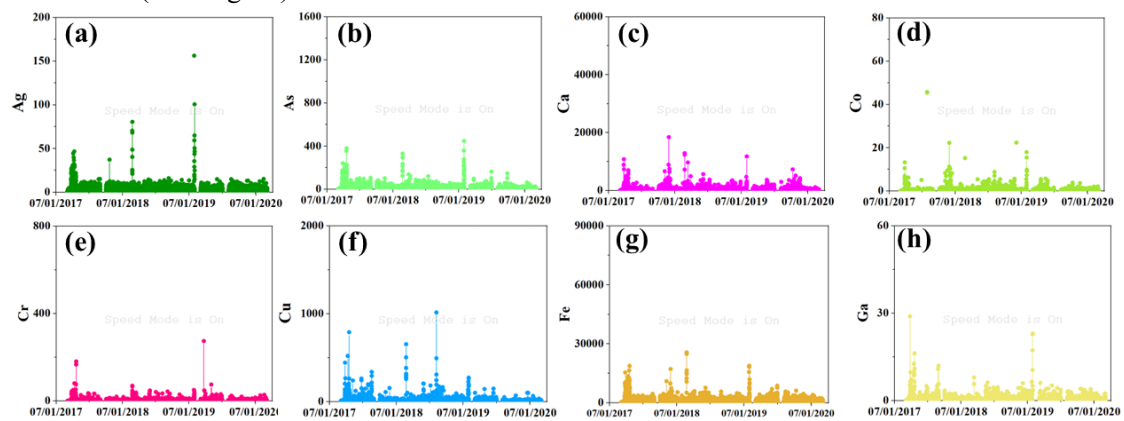
Figure S3 Time-series for Hg (a), K (b), Mn (c), Ni (d), Pb (e), Se (f), V (g), and Zn (h) during 2017-2020 (Unit: ng/m³).
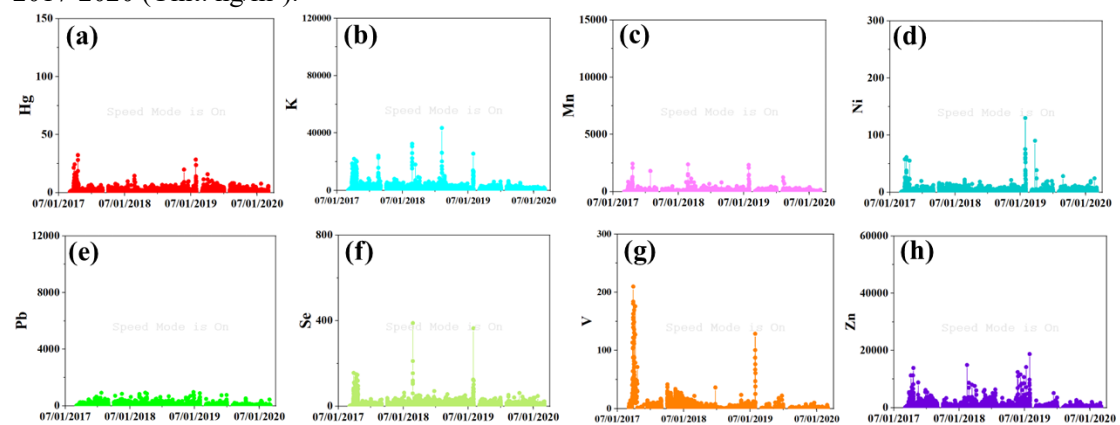
Figure S4 Performance of the random forest model in predicting the hourly concentrations of gaseous pollutants. The model was constructed with 80% of the original data and the remained data was used to validate the model. The black solid line denotes the best-fitting curve for all of the points, while the black dashed line represents the diagonal, which means the same observed and simulated values. (a)-(p) represent the predictive performances for Ag, As, Ca, Co, Cr, Cu, Fe, Ga, Hg, K, Mn, Ni, Pb, Se, V, and Zn, respectively (Unit: ng/m^3).
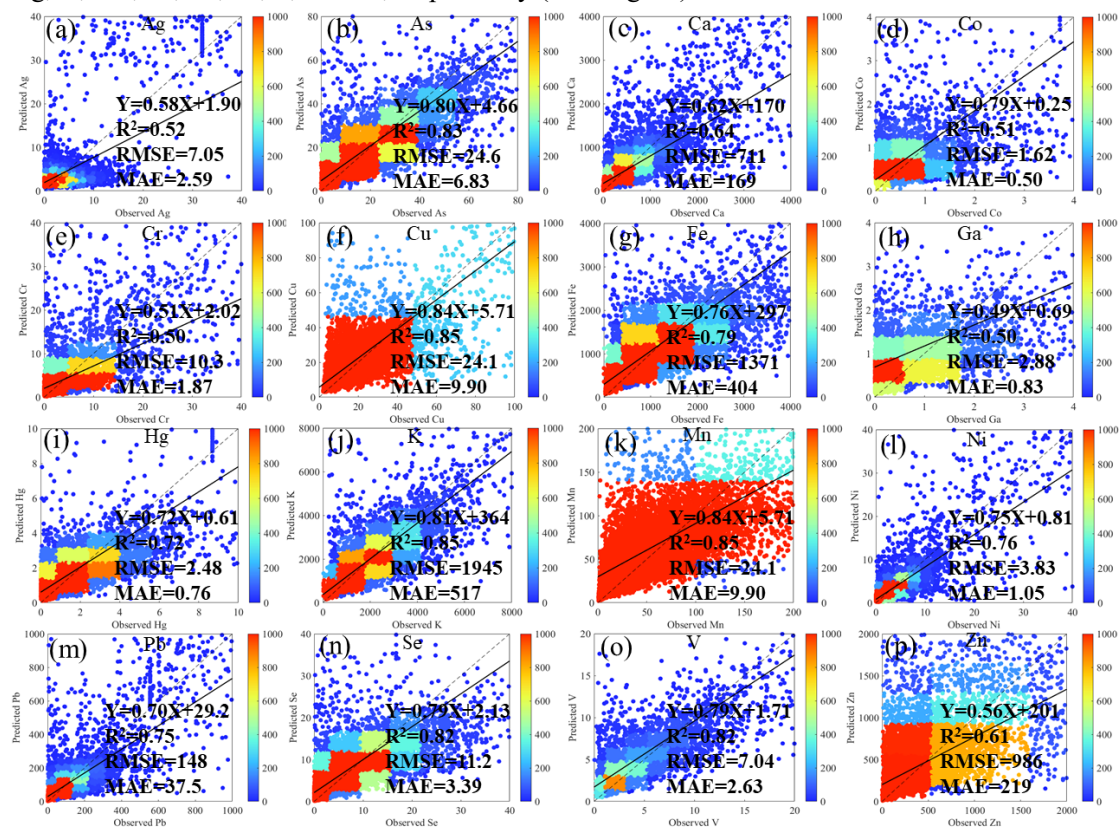
Figure S5 Changes in observed concentrations of trace elements from 2017 to 2020 against the changes derived from the emission and meteorological changes. The blue, orange, and green columns denote the original concentrations, emission-induced concentrations, and meteorology-induced ones, respectively.
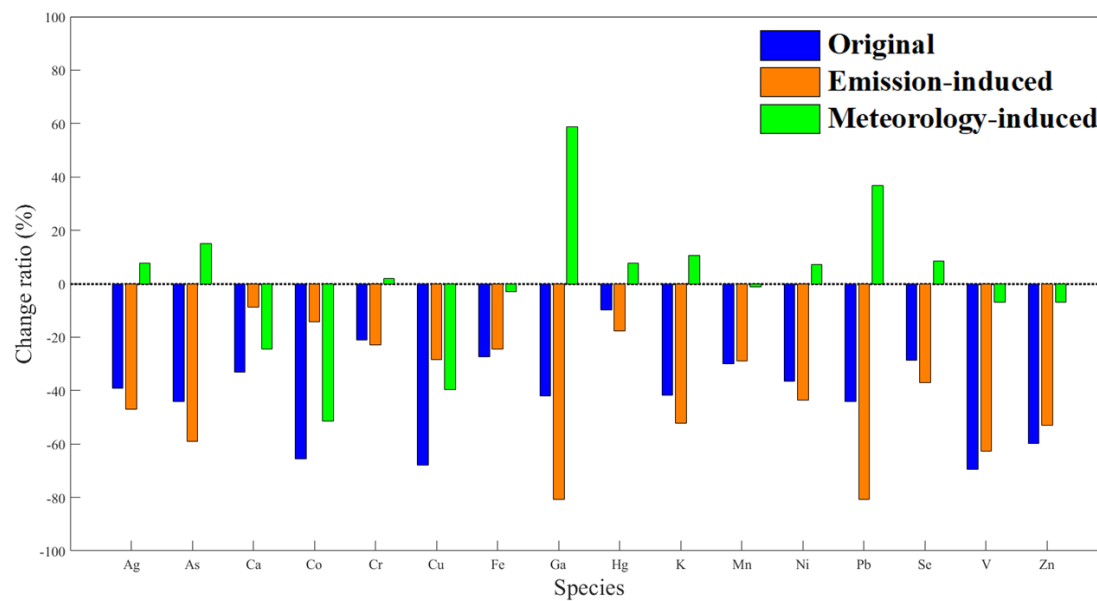
Figure S6 72-h backward trajectories arriving at Tangshan during biomass burning episodes in harvesting season (a). Polar plots of K concentration in Tangshan during 2017-2020 (b). The color bar denotes the K concentration (Unit: ng/m^3).
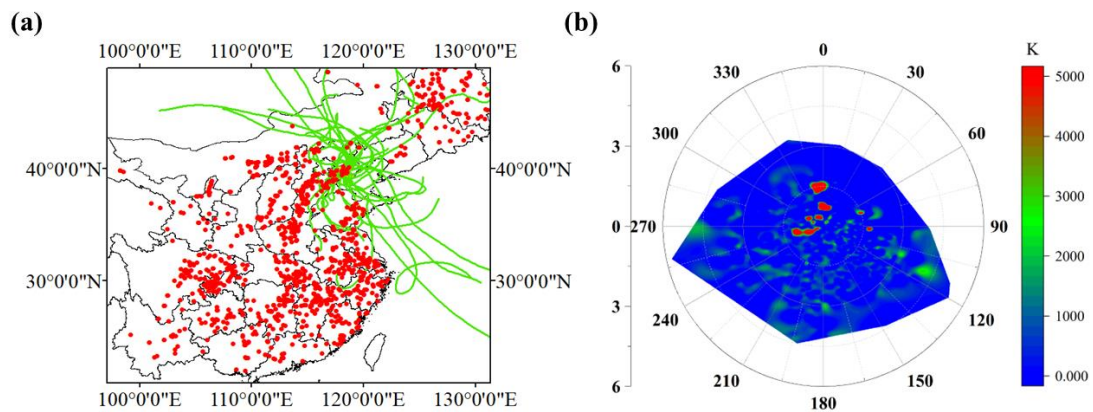
Figure S7 The 72-h air mass trajectories (a) and cluster result (b) in Tangshan during spring, 2018. The red, green, and blue solid line account for 16%, 55%, and 29% of the total air mass trajectories, respectively.
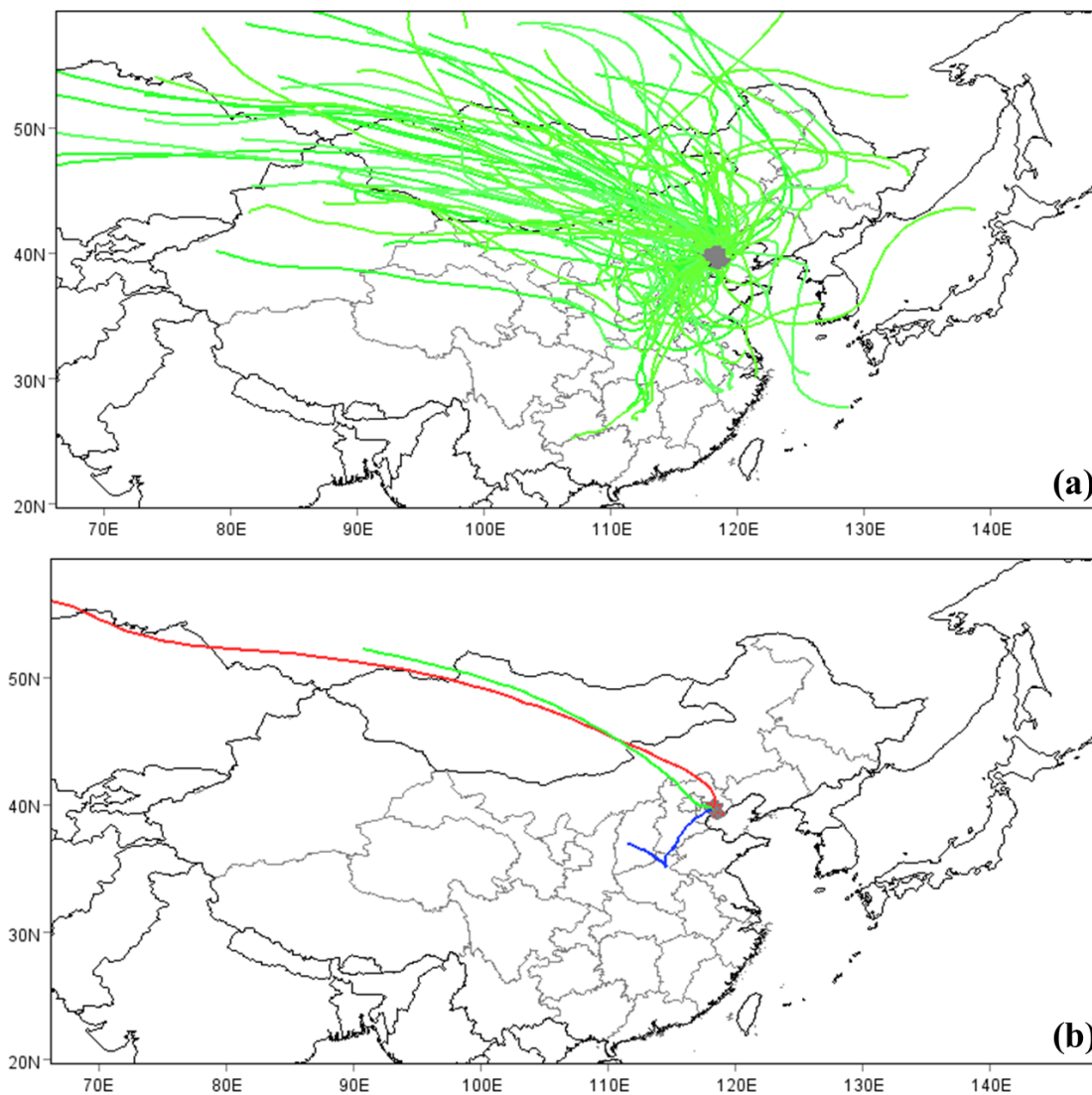
Figure S8 Polar plots of V (a) and Ni (b) in Tangshan during summer and autumn. The color bar reflects the concentrations of V and Ni (Unit: ng/m^3).
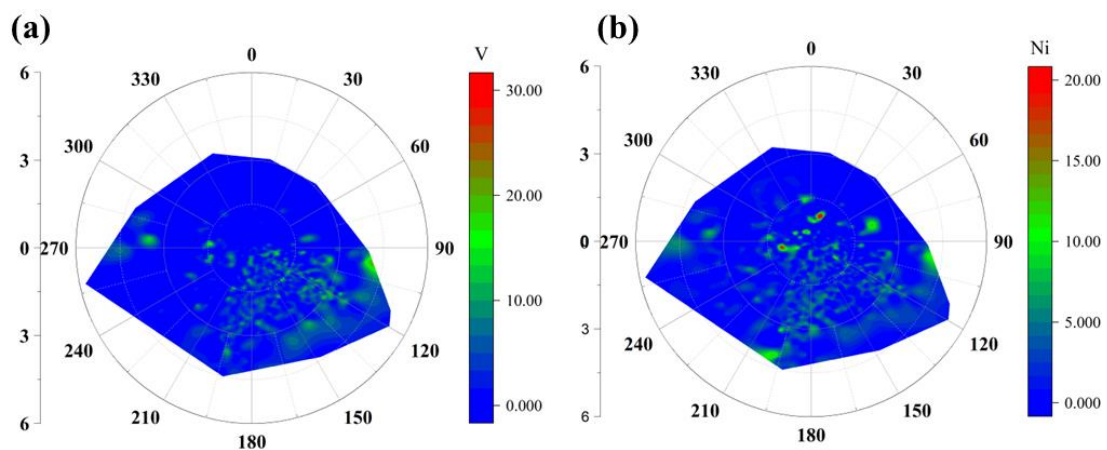
Figure S9 Source apportionment of trace elements in PM$_{2.5}$ during 2017-2020. Red, orange, green, blue, pink, and dark yellow bars denote the sources of biomass burning, non-ferrous metal smelting, coal combustion, ferrous metal smelting, heavy oil combustion, and traffic-related dust, respectively.
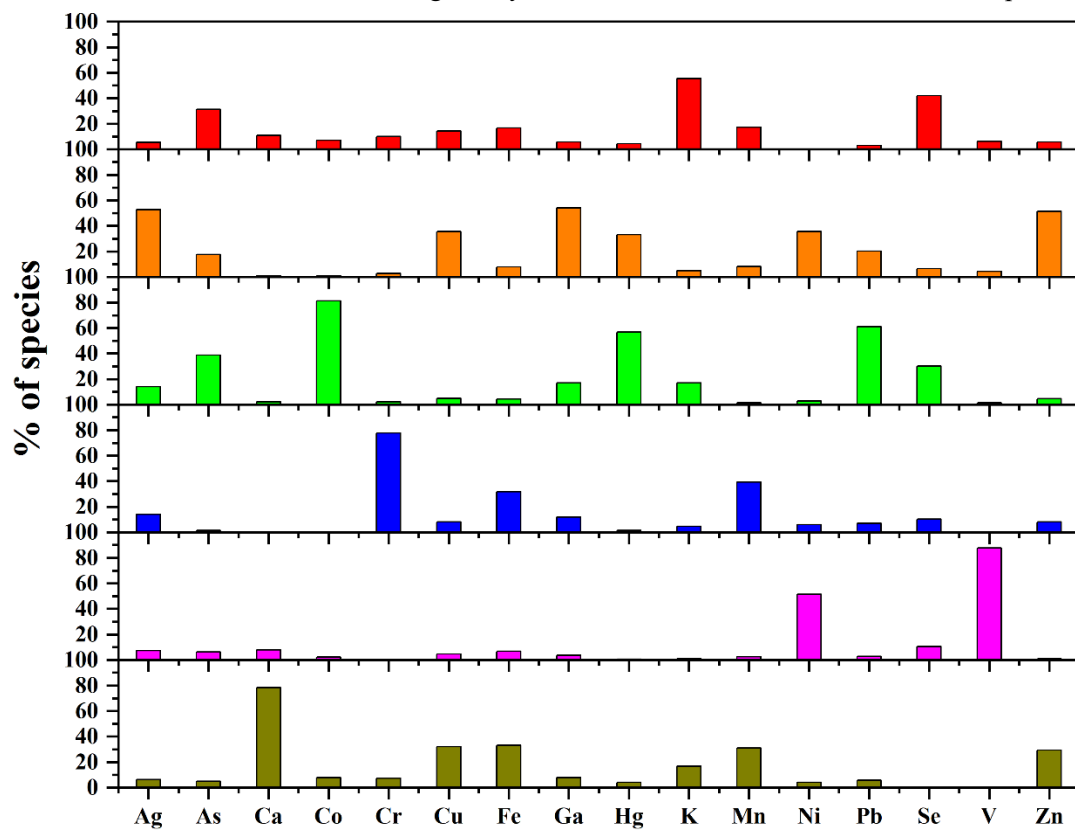
Figure S10 Diurnal variations of Ca, Fe, Cu, and Zn (ng/m^3) concentrations in Tangshan during 2017-2020.
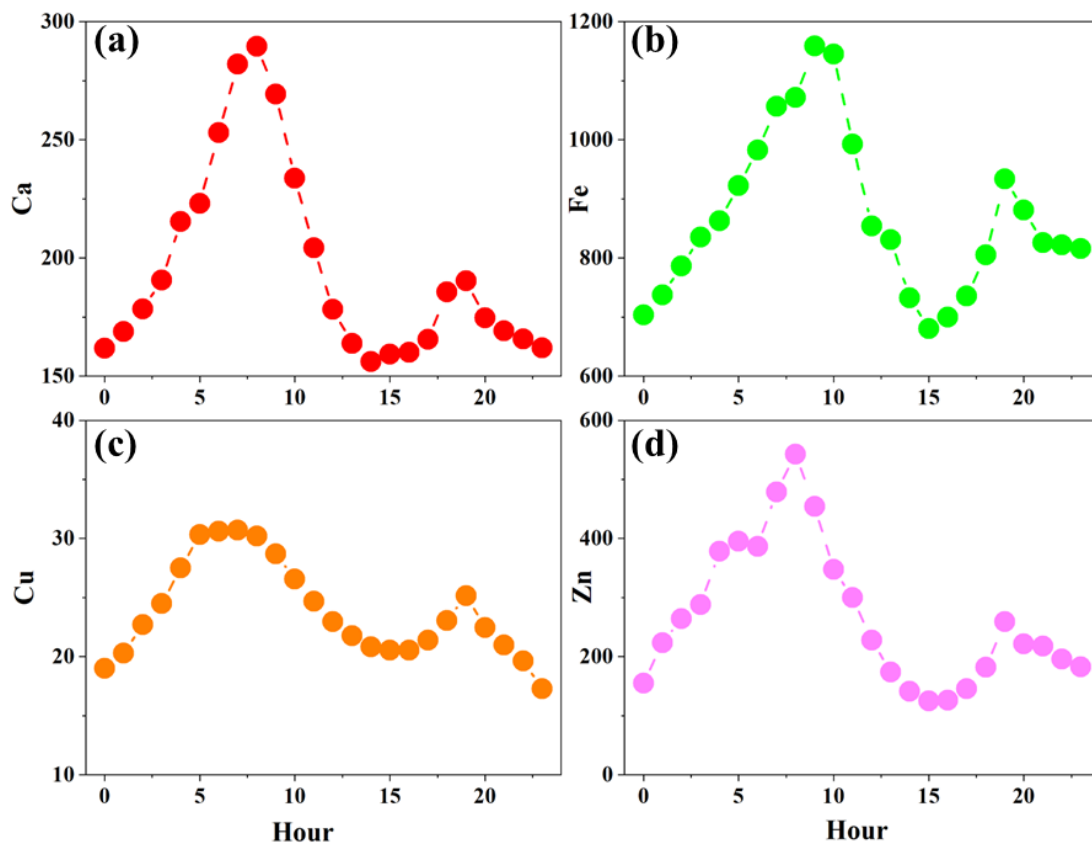
Table S1 Basic information and data sources of predictors for element estimation in this study.

| Dataset	Variable	Unit	Time resolution	Monitoring technique
Element	Ag	ng/m^3	Hourly	Model Xact 625
	As	ng/m^3	Hourly	Model Xact 625
	Ca	ng/m^3	Hourly	Model Xact 625
	Co	ng/m^3	Hourly	Model Xact 625
	Cr	ng/m^3	Hourly	Model Xact 625
	Cu	ng/m^3	Hourly	Model Xact 625
	Fe	ng/m^3	Hourly	Model Xact 625
	Ga	ng/m^3	Hourly	Model Xact 625
	Hg	ng/m^3	Hourly	Model Xact 625
	K	ng/m^3	Hourly	Model Xact 625
	Mn	ng/m^3	Hourly	Model Xact 625
	Ni	ng/m^3	Hourly	Model Xact 625
	Pb	ng/m^3	Hourly	Model Xact 625
	Se	ng/m^3	Hourly	Model Xact 625
	V	ng/m^3	Hourly	Model Xact 625
	Zn	ng/m^3	Hourly	Model Xact 625
Meteorology	T	°C	Hourly	sonic anemometer
	RH	%	Hourly	sonic anemometer
	WS	m/s	Hourly	sonic anemometer
	WD	°	Hourly	sonic anemometer
	P	hPa	Hourly	sonic anemometer
Time	Year	/	Hourly	/
	DOY	/	Hourly	/
	DOW	/	Hourly	/
	HOY	/	Hourly	/

Table S2 LOD (ng/m^3) of each element in PM$_{2.5}$ in our study determined by the Model Xact 625.

Element	LOD
K	1.18
Ca	0.56
V	0.15
Cr	0.14
Mn	0.13
Fe	0.73
Ni	0.20
Cu	0.19
Zn	0.23
As	0.11
Se	0.14
Ag	0.20
Ga	0.05
Co	0.05
Hg	0.19
Pb	0.22

Table S3 Sampling duration, analytical technique, and average concentrations of trace elements in different cities (Unit: ng/m^3).

	Tangshan	Beijing	Shanghai	Zibo	Chengdu	London	Toronto	Barcelona	Genoa	Venice	Athenes
References	Our study	(Cui et al., 2019)	(Chang et al., 2018)	(Zhang et al., 2018)	(Wang et al., 2018)	(Visser et al., 2015)	(Sofowote et al., 2014)	(Salameh et al., 2015)	(Salameh et al., 2015)	(Salameh et al., 2015)	(Grivas et al., 2018)
Sampling duration	2017-2020	2016-2017	2016-2017	2006-2007	2014-2015	11 Jan. to 14 Feb. 2012	1 Dec. 2010 to 30 Nov. 2011	20 Sep. to 20 Oct. 2010	Mar.–Sep. 2011	Jan.–Dec. 2011	May 2011 to Apr. 2012
Analytical technique	Model Xact 625	ED-XRF	ED-XRF	WD-XRF	ED-XRF	SR-XRF	ED-XRF	PIXE	ED-XRF	GFAAS	ED-XRF
Sampling site	Urban	Urban	Urban	Urban	Urban	Kerb side	Industry	Road side	Urban	Urban	Urban
K	1400	900	390	4180	720	27	27	89	100	433	241
Ca	330	493	190	1670	240	79	54	109	110	2044	397
V	4	1.1	13	8.2	1.9	1.3	0.1	9	14	11	5.8
Cr	2.8	3.6	4.5	20	5.6	2.3	0.2	8	--	30	1.8
Mn	54	37	32	100	34	4.8	1.8	7	4	91	4.8
Fe	880	738	410	1930	456	350	77	96	142	908	320
Ni	2.2	1.6	6	11	2.1	0.5	0.2	3	7	26	3.2
Cu	22	32	12	30	19	13	3.1	5	6	84	14
Zn	320	174	120	710	238	8.9	11	35	19	77	51
As	15	11	6.6	30	11	--	0.3	--	--	--	--
Se	6.5	4.1	2.6	20	--	--	--	--	--	--	--
Hg	1.5	2.5	2.2	--	--	--	--	--	--	--	--
Pb	58	65	27	420	55	2.3	2.4	17	6	41	14

Note. ED-XRF = energy dispersive X-ray fluorescence analysis, PIXE = particle-induced X-ray emission analysis, GFAAS = graphite furnace atomic absorption spectrometry, WD-XRF = wavelength dispersive X-ray fluorescence analysis, SR-XRF = synchrotron radiation-induced X-ray fluoresce analysis.

Table S4 Summary of PMF error diagnostics based on DISP.

Error Code:	0					
The largest decrease in Q:	0					
%dQ	0					

Swaps by Factor:	Biomass burning	Non-ferrous metal smelting	Coal combustion	Ferrous metal smelting	Heavy oil combustion	Traffic- related dust
dQmax=4	0	0	0	0	0	0
dQmax=8	0	0	0	0	0	0
dQmax=15	0	0	0	0	0	0
dQmax=25	0	0	0	0	0	0

Table S5 Summary of PMF error diagnostics based on BS.

BS Mapping (r≥0.6)	Biomass burning	Non-ferrous metal smelting	Coal combustion	Ferrous metal smelting	Heavy oil combustion	Traffic-related dust	Unmapped
Biomass burning and waste incineration	100	0	0	0	0	0	0
Non-ferrous metal smelting	0	100	0	0	0	0	0
Coal combustion	0	0	100	0	0	0	0
Ferrous metal smelting	0	0	1	98	1	0	0
Heavy oil combustion	0	0	0	0	100	0	0
Traffic- related dust	0	0	0	0	0	100	0

Table S6 Summary of PMF error estimation diagnostics from BS-DISP.

% of Cases Accepted:	98%					
Largest Decrease in Q:	-24					
%dQ	-0.01					
# of Decreases in Q:	1					
# of Swaps in Best Fit:	0					
# of Swaps in DISP:	1					
Swaps by Factor:	Biomass burning	Non-ferrous metal smelting	Coal combustion	Ferrous metal smelting	Heavy oil combustion	Traffic- related dust
dQ^{max}=0.5	0	0	1	0	0	0
dQ^{max}=1	0	0	1	0	0	0
dQ^{max}=2	0	0	1	0	0	0
dQ^{max}=4	0	0	1	0	0	0

Table S7 Recommended values of the parameters for health risk assessment of trace metals.

Parameter	Adult	Child	Unit
InhR	16.5	8.6	m^3/d
EF	365	365	d/a
ED	24	6	a
BW	70	15	kg
Cancer AT	70*365	70*365	d
Non-cancer AT	ED*365	ED*365	d

Table S8 Reference dose (RfD) (mg kg^{-1} d^{-1}) and cancer slope factor (CSF) (kg d mg^{-1}) of selected trace elements in references.

Element	RfD	CSF
Cr	3×10^{-3}	5×10^{-1}
Mn	1.4×10^{-1}	
Fe	7×10^{-1}	
Co	3×10^{-4}	
Ni	2×10^{-2}	
Cu	4×10^{-2}	
Zn	3×10^{-1}	
As	3×10^{-4}	1.5
Pb	2×10^{-2}	5×10^{-1}

References

Chang, Y., Huang, K., Xie, M., Deng, C., Zou, Z., Liu, S., and Zhang, Y.: First long-term and near real-time measurement of trace elements in China's urban atmosphere: temporal variability, source apportionment and precipitation effect, Atmos. Chem. Phys., 18, 11793-11812, 2018.

Cui, Y., Ji, D., Chen, H., Gao, M., Maenhaut, W., He, J., and Wang, Y.: Characteristics and sources of hourly trace elements in airborne fine particles in urban Beijing, China, J. Geophys. Res. Atmos., 124, 11595-11613, 2019.

Grivas, G., Cheristanidis, S., Chaloulakou, A., Koutrakis, P., and Mihalopoulos, N.: Elemental composition and source apportionment of fine and coarse particles at traffic and urban background locations in Athens, Greece, Aerosol Air Qual. Res., 18, 1642-1659, 2018.

Li, R., Guo, J. P., Geng, G. N., Xiao, Q. Y., and Zhang, Q.: Satellite-derived long-term estimates of full-coverage PM_1 concentrations across China based on a stacking decision tree model, Atmos. Environ., 255, 118448, 2021.

Ma, Z. W., Liu, R. Y., Liu, Y., and Bi, J.: Effects of air pollution control policies on $PM_{2.5}$ pollution improvement in China from 2005 to 2017: a satellite-based perspective, Atmos. Chem. Phys., 19, 6861–6877, 2019.

Salameh, D., Detournay, A., Pey, J., Pérez, N., Liguori, F., Saraga, D., Bove, M. C., Brotto, P., Cassola, F., Massabò, D., Latella, A., Pillon, S., Formenton, G., Patti, S., Armengaud, A., Piga, D., Jaffrezo, J.L., Bartzis, J., Tolis, E., Prati, P., Querol, X., Wortham, H., and Marchand, N.: $PM_{2.5}$ chemical composition in five European Mediterranean cities: A 1-year study, Atmos. Res., 155, 102-117, 2015.

Sofowote, U. M., Rastogi, A. K., Debosz, J., and Hopke, P. K.: Advanced receptor modeling of near-real-time, ambient $PM_{2.5}$ and its associated components collected at an urban-industrial site in Toronto, Ontario, Atmos. Pollut. Res., 5, 13-23, 2014.

Visser, S., Slowik, J., Furger, M., Zotter, P., Bukowiecki, N., and Dressler, R.: Kerb and urban increment of highly time-resolvedtrace elements in PM_{10}, $PM_{2.5}$, and $PM_{1.0}$ winter aerosol in London during ClearfLo 2012, Atmos. Chem. Phys., 15(5), 2367-2386. https://doi.org/10.5194/acp-15-2367-2015, 2015.

Wang, Q., Qiao, L., Zhou, M., Zhu, S., Griffith, S., Li, L., and Yu, J. Z.: Source apportionment of $PM_{2.5}$ using hourly measurements of elemental tracers and major constituents in an urban environment: investigation of time-resolution influence, J. Geophys. Res. Atmos., 123, 5284-5300, 2018.

Zhang, J., Zhou, X., Wang, Z., Yang, L., Wang, J., and Wang, W.: Trace elements in $PM_{2.5}$ in Shandong Province: source identification and health risk assessment, Sci. Total Environ., 621, 558-577, 2018.